# Pseudomorphic growth of Fe monolayers on Ir(001)-(1×1): From a fct precursor to a bct film

V. Martin, W. Meyer, C. Giovanardi, L. Hammer, and K. Heinz
*Lehrstuhl für Festkörperphysik, Universität Erlangen-Nürnberg, Staudtstrasse 7, D-91058 Erlangen, Germany*

Z. Tian, D. Sander, and J. Kirschner
*Max-Planck-Institut für Mikrostrukturphysik, Weinberg 2, D-06120 Halle/Saale, Germany*

(Received 3 August 2007; revised manuscript received 11 October 2007; published 14 November 2007)

The epitaxial growth of Fe monolayers on the unreconstructed Ir(001) surface was investigated experimentally by determining film structure, morphology, stress, and magnetism. Our combined quantitative low energy electron diffraction (LEED) and cantilever stress results indicate pseudomorphic Fe growth with a constant in-plane film strain in an almost perfect layer-by-layer growth mode from 0–10 layers. The combination of the structural analysis by LEED with stress measurements suggests that the first two layers of Fe grow as a face-centered tetragonally (fct) distorted precursor. Further deposition of Fe leads to the growth of a body-centered tetragonally distorted phase on top of the fct precursor, which retains its structure. The magneto-optical Kerr effect reveals that the Fe film is ferromagnetic with an in-plane easy magnetization direction along Fe⟨100⟩.

DOI: 10.1103/PhysRevB.76.205418 PACS number(s): 68.03.Cd, 68.55.−a, 68.55.Ac, 75.70.Ak

## I. FOCUS

The pseudomorphic growth, i.e., the epitaxial growth of films with the same in-plane lattice parameter as the substrate, has attracted a lot of experimental and theoretical attention in the past.[1] This enduring interest in pseudomorphic growth is also due to the possibility to investigate the impact of lattice strain, which results from the epitaxial misfit between film and substrate, on film structure, morphology, and magnetism. Strains as high as several percent, far above the elasticity limits of even high strength materials, are frequently encountered in pseudomorphic systems, where they often induce magnetic properties which deviate sharply from the respective bulk behavior.[2]

A particularly interesting film material is iron due to its intimate correlation between structural and magnetic properties.[3] It is well known that iron exhibits a rather rich variety of structural and magnetic phases, in particular, when its lattice is—as realized in epitaxially strained films—tetragonally distorted, where it loses the cubic symmetry of its body-centered-cubic (bcc) or face-centered-cubic (fcc) bulk reference state. A number of theoretical papers concentrate on such tetragonal phases as function of the lattice parameter, in most cases for (artificial) bulk material (e.g. Refs. 4–9).

Epitaxial iron films on fcc(001) substrates were studied intensively, and also different magnetic phases of fcc-type iron have been identified. The fcc(001) substrates investigated up to date include Ag,[10–12] Ni[13,14] as well as Ni/Cu,[15] Pd,[16,17] Rh,[18,19] Au,[20–22] $Cu_3Au$,[23–26] $Cu_{64}Al_{16}$,[27] and, last but not least, the most frequently used substrate, Cu, for which a large number of papers exist. We refer to recent reviews and references therein.[1,28]

The most interesting result of some of these previous studies is the thickness dependent martensitic transition of Fe from a fct phase at low film thickness to a bct phase at higher thickness. It has been shown that this structural transition drives a corresponding change of the magnetic properties of the Fe film.[29]

We introduce Ir(001) as an interesting substrate to study Fe growth on a fcc(001) substrate. Its in-plane lattice parameter $[a_{\parallel}=a(\mathrm{Ir})/\sqrt{2}=2.715\ \text{Å}]$ is right in between the corresponding parameters for bcc-Fe (2.866 Å) and fcc-Fe (2.527 Å). Additionally, it offers some beneficial properties with respect to other substrates. Our results indicate that there is no intermixing between Fe and Ir, even at slightly elevated temperatures around 400 K. This ensures atomically sharp interfaces, which allow for reliable structural and stress analyses. The Fe growth leads to very flat films, indicative of an almost perfect layer-by-layer growth. Again, this makes the structural and stress analyses straightforward, without the need to take strain relaxations and roughness into account. Finally, the growth of Fe films thicker than two layers leads to body-centered tetragonally (bct) distorted Fe with (001) orientation. This contrasts with the bcc(011) domains, which form on Cu(001) at higher Fe thickness. The existence of just one structural domain of bct Fe facilitates both structural and stress analyses. The drawback of the Ir(001) substrate is that the growth of face-centered tetragonally (fct) distorted Fe is limited to the first two layers. We find that the subsequent deposition of Fe leads to a bct Fe film, which grows on top of the fct phase.

The most important result of our study is that we find clear cut experimental evidence from quantitative low energy electron diffraction (LEED) data and stress measurements that Fe films between 0–10 ML (monolayer) are pseudomorphically strained. Above 2 ML, a bct Fe structure results, where our magneto-optical Kerr-effect (MOKE) studies reveal ferromagnetic order with an easy in-plane magnetization direction for films of 4 ML and thicker. The measured compressive film stress (−10 GPa) in this thickness range is in agreement with the compressive lattice misfit for bcc Fe on Ir(001). Thinner films are also pseudomorphically strained, but here a tensile film stress is measured. These results lead us to propose that the first two Fe monolayers are grown in a fct phase.

 

## II. SAMPLE PREPARATION AND APPLIED METHODS

The stable surface structure of Ir(001) is the Ir(001)-$(1\times5)$ quasihexagonal reconstruction. The top layer accommodates—by a quasihexagonal and buckled atomic arrangement—20% more atoms than subsurface layers.[30,31] Deposition of iron on this surface beyond a coverage of about 0.25 ML (1 ML corresponds to one adatom per quadratic surface unit cell, giving an atomic surface density of $1.357\times10^{15}$ cm$^{-2}$) lifts the quasihexagonal reconstruction. Thereby the 20% extra iridium atoms of the former reconstructed layer are expelled to form a new surface layer where they mix with iron atoms.[32,33] The top layer is corrugated due to the different atomic radii of the elements, and, as a consequence, a vertical modulation is imprinted on further deposited iron layers.[32]

In order to avoid both the corrugation and the intermixing at the Ir-Fe interface, we prepare the unreconstructed phase Ir(001)-$(1\times1)$. Though this phase is only metastable, it is effectively stationary at room temperature and below. It is prepared by lifting the hexagonal surface reconstruction by oxygen adsorption and subsequent exposure to hydrogen, which reacts with oxygen. The following desorption of the reaction products leaves a clean $(1\times1)$ surface behind.[34–36] A corresponding LEED pattern and scanning tunneling microscopy (STM) image are shown in Fig. 1.

Fe was deposited onto the Ir-$(1\times1)$ surface at 90 K at a deposition rate of 0.7 ML/min (deposition at about 300 K leads to an increased roughness of films with thicknesses higher than 5 ML). Fe was evaporated from a highly purified Fe rod (purity $>99.99\%$) with an electron beam evaporator at a pressure below $2\times10^{-10}$ mbar. The sample was annealed at about 420 K for 2 min after Fe deposition. Then, it was cooled again to 90 K and put in front of a home-made three-grid rear-view LEED optics for the structural analysis. During measurement, the pressure was typically $6\times10^{-11}$ mbar (with the reading of the Bayard-Alpert gauge uncorrected).

The entire diffraction pattern was acquired at normal incidence of the primary beam by a 12 bit digital charge coupled device camera operated under computer control.[37] These LEED intensity measurements were performed for electron energies between 50 and 600 eV, in steps of 0.5 eV. At each energy, eight images were averaged and stored. The whole data acquisition procedure took less than 15 min. Spot intensities were extracted by off-line evaluation of the stored data. At each energy, the spot under consideration was enframed by an electronic window, and the intensity signal within was added up pixel by pixel. The result was corrected for background intensities, as determined at the window edges, and finally the intensity was normalized with respect to the primary beam current. The resulting intensity vs energy spectra, $I(E)$, were averaged for symmetrically equivalent spots and slightly smoothed when necessary. The total energy width of the database, i.e., the energy width accumulated with respect to the energy range of eight symmetrically nonequivalent beams, was $\Delta E\approx2600$ eV.

The structural evaluation of the LEED $I(E)$ spectra was achieved by full dynamical intensity calculations. For the test of Fe-Ir intermixing at the interface, the perturbation method tensor LEED using the TENSERLEED program,[38] in particular, the version of chemical tensor LEED,[37] was applied. Scattering phase shifts up to an angular-momentum quantum number $l_{max}=13$ were used for both elements. Multiple scattering within layers was computed by matrix inversion, and the layers were stacked by the layer doubling method.[39] The optical potential accounting for electron attenuation, $V_{0i}$, was varied in the range 4–7 eV. Due to the electron energy extending up to 600 eV, an energy-dependent real part of the inner potential specific to each film was used, $V_{0r}=V_{00}+V_{01}(E)$ as taken from the literature[40] and with $V_{00}$ also varied in the course of the structural search. For the latter, an automated procedure using a frustrated simulated annealing method[41] controlled by the Pendry *R* factor[42] was applied. The latter's variance, $\mathrm{var}(R)=R_{min}\sqrt{8V_{0i}/\Delta E}$ with $R_{min}$ the minimum *R* factor achieved, was used for the error estimation of the model parameters. These parameters include the first five vertical spacings $d_{i,i+1}$ between layers $i$ and $i+1$ (independent of the chemistry of the layers involved) as well as the vibrational amplitudes (assumed to be isotropic) in the top two layers and, for thicker films, in their bulklike layers.

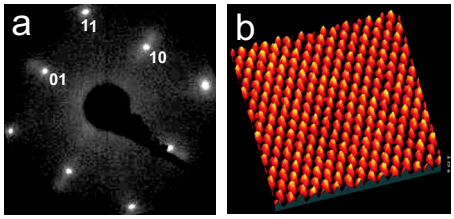


FIG. 1. (Color online) (a) LEED pattern at 100 eV with the beam notation of the reciprocal unit cell indicated and (b) atomically resolved STM image ($50\times50$ Å$^2$ taken at $U=2.75$ meV and $I=10.1$ nA) of the unreconstructed and metastable Ir(001)-$(1\times1)$ phase.

The sample had to be transferred (within UHV) to a second stage of the same vessel for STM measurements with a beetle-type STM, operated at room temperature. The iron films were imaged at positive sample bias. There was no pronounced voltage dependence of the image contrast.

Stress and MOKE measurements were carried out in a second UHV chamber, which was also equipped with facilities for computer-controlled LEED data acquisition. Thus, we use LEED $I(E)$ data as a transfer standard for both chambers to ensure a well defined and reproducible substrate and film preparation.

We used an optical two-beam cantilever deflection technique to determine the stress-induced curvature of a thin (0.1 mm) Ir single crystalline substrate (length: 12 mm; width: 2.5 mm), as described elsewhere.[43]

Fe was deposited onto the front surface of the Ir substrate held at 300 K, and the Fe film stress $\tau_F$ was deduced from the slope of the curve $(\tau_F t_F)$ as a function of film thickness $t_F$. A positive (negative) slope indicates tensile (compressive) stress. The Fe growth rate was of the order of 1 ML/min. It was determined from medium energy electron diffraction intensity oscillations, which were measured during film growth.[44]

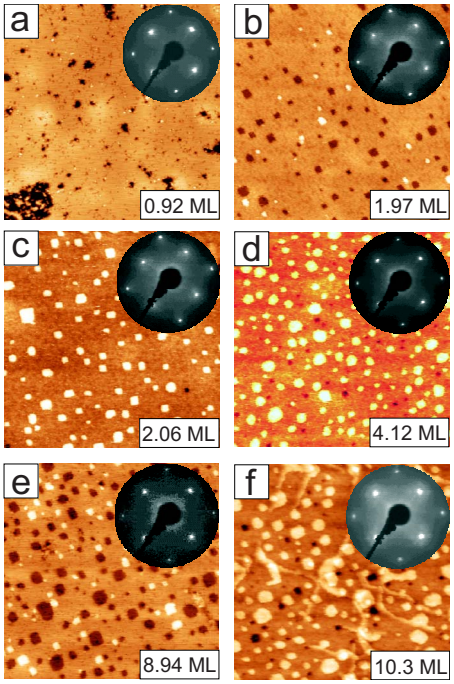


FIG. 2. (Color online) Selection of STM images ($1000 \times 1000$ Å$^2$) for increasing Fe coverage [the respective voltage (current) values in units of V (nA) are (a) 0.51 (0.49), (b) 1.4 (5.5), (c) 0.31 (0.92), (d) 0.085 (0.39), (e) 2.5 (0.24), and (f) 0.38 (0.58)]. The LEED patterns displayed as inset in each case were taken at 121 eV.

## III. RESULTS

### A. Morphology and structure of the Fe films by scanning tunneling microscopy and low energy electron diffraction

A selection of STM images taken at various Fe coverages is displayed in Fig. 2. The corresponding LEED patterns are shown as inset. The STM images reveal at most only three height levels at each coverage (except the highest one), i.e., holes (dark), extended flat areas (gray and/or red), and islands (bright). STM line profile measurements show that the holes have a depth of about 1.4–1.6 Å and the islands a height of about 1.5–1.6 Å, i.e., values close to the interlayer spacing of $\alpha$–Fe(100) (1.44 Å). The exact coverage in each case was evaluated from the images subtracting from a full $n$ ML coverage the fraction of holes in this layer and adding the fraction of iron in the layer $(n+1)$. These values are given in the different panels of Fig. 2.

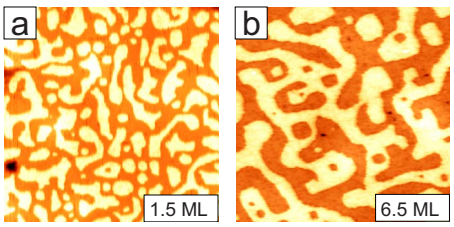


FIG. 3. (Color online) STM images ($1000 \times 1000$ Å$^2$) for coverage values of (a) 1.5 ML ($U$=0.40 V, $I$=0.82 nA) and 6.5 ML Fe ($U$=0.38 V, $I$=0.30 nA).

The STM image for 1.97 ML reveals that only very close to the full monolayer coverage do small islands in the third layer start to grow ($\approx 1\%$). At 1.95 ML (not shown), only a few such islands are found ($<0.5\%$). Also, as apparent from the image at 2.06 ML, already slightly above the full ML coverage, almost all holes in the first layer are filled. Apparently, as these features hold also for other near integer coverage values, there is almost ideal layer-by-layer growth. This is rather surprising given the substantial misfit between film and substrate. Consistently, at half-order numbers $(n+1/2)$ of coverage, there are practically no holes in the already completed $n$th layer and no islands on layer $(n+1)$ as displayed for two examples in Fig. 3.

LEED indicates a strictly pseudomorphic growth, as the LEED patterns are of $(1 \times 1)$ symmetry for all coverage values below 10 ML, and the spot positions are—within the error limits of measurement ($\approx a_{\|}/100$)—exactly at those of the clean Ir(001) substrate. It is also surprising that the quality of the epitaxial layer-by-layer growth does not degrade much up to about 10 ML, as evidenced by the sharp LEED pattern with low background intensity. Near and above this coverage, however, extra features develop in both the STM images and LEED patterns, see panel for 10.3 ML. We ascribe these extra features to the onset of strain relaxation due to the formation of misfit dislocations.

The connection between these structural changes around 10 ML Fe thickness and stress relaxation is further corroborated by our stress measurements, as discussed below.

### B. Structural analysis

Structural LEED intensity analyses were carried out for 1, 2, 4, and 9 ML Fe; the analysis of the clean Ir(001) surface was available from earlier work.[31] For all films, an excellent fit between experimental and model intensities could be achieved, as indicated by the respective $R$ factors $R$=0.097, 0.120, 0.129, and 0.157 (given for increasing film thickness). Figure 4 illustrates the excellent agreement between measured and calculated LEED spectra. From this agreement, we conclude that our structural model, which is the basis of the calculation, is valid. The resulting interlayer spacings are given in Fig. 5. The error estimation based on the variance of the $R$ factor gives an error of typically 0.01 Å for the first spacing, nearest to the vacuum interface. The error increases for deeper spacings and reaches the order of 0.03 Å for the fifth spacing. The reader should note already at this point that the 9 ML film exhibits an expansion of its top two layer spacings as compared to the spacings of deeper layers. We postpone the discussion of this point and of the overall structural results to Sec. IV.

Our structural analysis of the 1 ML film is also sensitive to intermixing between Fe and Ir. The best fit between the experimental data and the calculated model intensities was exactly at 100% Fe in the top layer. Though the related error margin is about 15%, we take that as a strong indication that there is no intermixing at the interface. Similar tests for intermixing were not applied for thicker Fe films.

### C. Film stress and magnetism

Figure 6 shows the stress change during the deposition of 12.5 ML Fe on Ir(001)-$(1 \times 1)$ at 300 K. The first 0.5 ML Fe

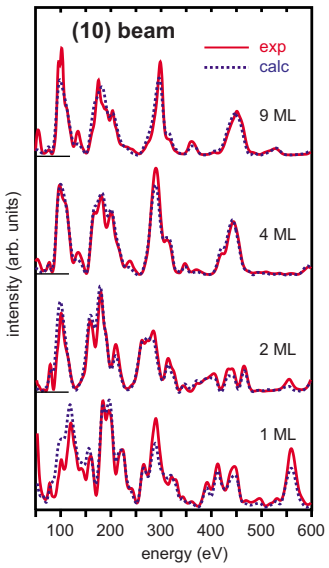


FIG. 4. (Color online) Experimental and calculated best-fit LEED spectra for the (10) beam of Fe films as indicated.

induces a compressive stress change of −1 N/m. Then, a positive slope of the stress curve is observed, which reaches +6 GPa around 1.5 ML. At 2 ML, the stress curve changes its slope again and continues with a negative slope. At 6 ML, a compressive film stress of −10 GPa is measured. With increasing deposition, the stress curve levels off from its constant slope around 10 ML. This stress relaxation is indicated by the deviation of the data points from the broken line, which indicates a stress of −10 GPa. Note that although Fe deposition continues, there is no appreciable cantilever stress change above 11 ML.

The most important result from our stress measurements is that we identify two stress regimes with opposite signs of

| clean Ir(001) | 1 ML Fe | 2 ML Fe | 4 ML Fe | 9 ML Fe |
|---|---|---|---|---|
| | | | | 1.59 |
| | | | | 1.58 |
| | | | | 1.55 |
| | | | 1.55 | 1.54 |
| | | | 1.59 | (1.56) |
| | | | 1.58 | (1.56) |
| | | 1.64 | 1.61 | |
| | 1.69 | 1.77 | 1.76 | |
| 1.85 | 1.96 | 1.93 | 1.94 | |
| 1.94 | 1.91 | 1.91 | 1.92 | |
| 1.92 | 1.92 | 1.93 | (1.92) | |
| 1.93 | 1.92 | (1.92) | (1.92) | |
| (1.92) | (1.92) | (1.92) | (1.92) | |

FIG. 5. Interlayer spacings (in Å) for the clean Ir(001) surface as taken from earlier work (Ref. 31) and for the Fe films of the four thickness values as given. Parentheses indicate that the spacings were not independently varied but assumed to be equal (also for deeper layers).

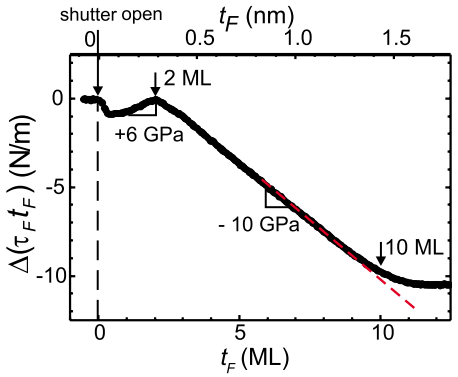


FIG. 6. (Color online) Cantilever stress change $[\Delta(\tau_F t_F)]$ measured during the deposition of Fe on Ir(001)-$(1\times1)$ at 300 K. The slope of the curve at 1.5 and 6 ML indicates film stresses of +6 and −10 GPa, respectively. The deviation of the stress curve from the latter slope indicates a stress relaxation, starting around 10 ML.

film stress. Films thinner than 2 ML are under tensile stress, whereas films thicker than 2 ML are under compressive stress. As will be discussed below, these results suggest a pseudomorphically strained bct Fe film in the region of compressive stress, whereas the tensile stress is ascribed to a fct Fe film.

The initial compressive stress change for submonolayer Fe deposition is typical for a change of surface stress of the substrate upon adsorption. The clean Ir surface is under large tensile surface stress, and the deposition of Fe relaxes the surface stress giving rise to a compressive stress change. Similar surface stress relaxation has been measured for deposition of 3*d* elements on W and are ascribed to the adsorbate-induced reduction of the large tensile surface stress of the substrate.[45,46] This surface stress change shifts the stress curve by −1 N/m, and its discussion goes beyond the scope of the present work.

The stress relaxation above 10 ML corroborates directly the above statement on the formation of misfit dislocation, which was based on the STM and LEED data of the 10.3 ML film.

MOKE measurements have been performed *in situ* with the stress measurements to study the magnetic properties of the Fe films on Ir(001)-$(1\times1)$. The MOKE signal is measured at 300 K in a magnetic field oriented within the film plane along Ir⟨110⟩, i.e., parallel to Fe⟨100⟩. We obtain hysteresis curves with a coercivity of 12 mT and almost full remanence at zero field for Fe films thicker than 5 ML. This indicates ferromagnetic behavior with an easy in-plane magnetization direction along Fe⟨100⟩, which is also the easy magnetization direction of bulk bcc Fe. Presently, experimental modifications are performed to extend the MOKE measurements to lower temperature and higher magnetic fields for a characterization of thinner Fe films.

## IV. DISCUSSION

Before we discuss our results in view of the impact of lattice strain on the film structure, it is important to agree

TABLE I. Lattice constants $a$ in Å from Ref. 47, epitaxial misfit $\epsilon_{\|}=(a_{\|,film}-a_{\|,bulk})/a_{\|,bulk}$, calculated strain along the film normal $\epsilon_{33}=-2\epsilon_{\|}c_{12}/c_{11}$, elastic constants $c_{ij}$ in GPa from Ref. 48, Young's modulus $Y=(c_{11}+2c_{12})(c_{11}-c_{12})/(c_{11}+c_{12})$ in GPa, and Poisson's ratio $\nu=c_{12}/(c_{11}+c_{12})$. For a discussion of these quantities, see Ref. 2.

| | $a$ | $\epsilon_{\|}$ | $\epsilon_{33}$ | $c_{11}$ | $c_{12}$ | $c_{44}$ | $Y$ | $\nu$ |
|---|---|---|---|---|---|---|---|---|
| Ir | 3.839 | | | 600 | 260 | 270 | 443 | 0.302 |
| Fe, bcc | 2.866 | −0.053 | +0.062 | 230 | 134 | 116 | 131 | 0.368 |
| Fe, fcc[a] | 3.574 | +0.074 | −0.099 | 200 | 134 | 92 | 92 | 0.401 |

[a]Data for fcc-Fe have been obtained for bulk fcc-Fe at high temperature (Refs. 41 and 49). The tabulated values are extrapolated to 300 K. The thermal expansion of fcc Fe is taken as $8.5\times10^{-5}$ Å/K. The $c_{ij}$ are extrapolated to 300 K, assuming the same temperature dependence as given for bcc Fe (Ref. 50). Thus, the high temperature data for fcc-Fe (Ref. 49). $c_{11}$, $c_{12}$, and $c_{44}$ are increased by 30%, 10%, and 20%, respectively.

upon proper reference values for both the lattice parameter and the elastic properties of Fe in its bcc and fcc modifications. Table I compiles reference data for the system Fe on Ir. Note that the fcc Fe data originate from measurements performed for bulk $\gamma$-Fe, which were taken at high temperature. We extrapolated these values to 300 K, as described in the table caption, to make contact with our measurements.

In the following, we begin with the discussion of a thick Fe film (9 ML). It is found to grow as a bct phase on top of the layers at the interface, which appear as a fct precursor as discussed subsequently. The distinction between bct and fct is justified and based upon the opposite signs of film stress, which changes from compressive in the bct phase to tensile in the fct-type phase.

### A. Structure and stress of thicker Fe films

A detailed structural analysis has been performed for the 9 ML thick Fe film. The quantitative LEED analysis gives an average layer spacing of 1.55 Å for the bulk of the film (leaving out the top two spacings which are relaxed, see Fig. 5). The in-plane lattice spacing of the Fe film is, due to the pseudomorphic growth on Ir, fixed at $a_{\|}=a_{\mathrm{Ir}}/\sqrt{2}=2.715$ Å. Can we already decide from these numbers alone whether the 9 ML film originates from the bcc or from the fcc phase? The answer is no.

The difference between a bcc and a fcc structure can be expressed by the ratio of the vertical lattice constant $c$ over the in-plane lattice constant $a_{\|}$. An undistorted fcc material has $c/a=\sqrt{2}$, whereas an undistorted bcc material has $c/a=1$. For our example of the 9 ML Fe film, $c$ equals twice the layer spacing resulting in $c/a=1.142$. This ratio fits neither the bcc nor the fcc value. It is halfway between both values, and no decision is possible.

So, we need to decide *a priori* which reference state to take for the equilibrium lattice constant of the Fe film in order to treat the impact of lattice strain on the layer spacing. Our decision defines the in-plane lattice misfit $\epsilon_{\|}$ and is only justified if it gives a reasonable description of both the vertical layer spacing and the proper film stress for the given in-plane lattice constant. We employ continuum elastic theory to calculate the out-of-plane lattice strain $\epsilon_{33}$ from the in-plane lattice misfit $\epsilon_{\|}$. The result is given in Table I for both fcc and bcc Fe.

For bcc Fe, we obtain a reasonable agreement between calculated and measured layer spacings and stresses. The in-plane compressive lattice misfit of bcc Fe deposited on Ir(001) is $\epsilon_{\|}=-0.053$, and this induces a vertical expansion of the layer spacing to $(1+\epsilon_{33})0.5a_{\mathrm{Fe},bcc}=1.522$ Å. The film stress follows as $\tau_F=Y/(1-\nu)\epsilon_{\|}=-11$ GPa. Both values are in reasonable agreement with the measured average layer spacing of 1.55 Å and the experimental stress of −10 GPa. We conclude that the 9 ML Fe film can be regarded as a bct phase of Fe, whereby the first two layers at the Ir interface are a fct precursor (see below).

Note that the fcc reference state would lead to a tensile film stress of +11.4 GPa and a layer spacing of 1.61 Å. The stress value is in sharp contrast to the experimental data of the thicker film, and the deviation of the layer spacing is larger than for the bct case. However, for the thinner films, the fcc reference gives the better agreement with the experimental data, as will be discussed below.

Evidently, continuum elasticity theory applied to bulk Fe is appropriate to identify the film structure as either fct or bct. This might come as a surprise, as it is not clear why bulk reference data on both lattice spacing and elastic constants should also work for a few monolayers. However, our results presented here and our previous work on other systems provide compelling evidence that continuum elasticity can provide very reasonable description of film stress and layer relaxation for pseudomorphic films thicker than 2 ML.[44,51–53]

Concerning Fe films, recent calculations for unsupported Fe slabs have shown that with decreasing slab thickness, the lattice constant decreases and, in fact, also the elastic constants are modified.[54] However, for our film thickness of about 14 Å, the modifications of both the lattice parameter and the elastic constants are reported to be rather small, that is, the treatment of the film as bulk material appears to be a good approximation. Also, the calculations of the epitaxial stress along the epitaxial Bain path (EBP) as function of the epitaxial strain (Fig. 3 in Ref. 54) yield a value of $\sigma_{\|}\approx-9.6$ GPa for the strain of our Fe/Ir film, $\epsilon_{\|}^{bct}=-5.3\%$. This not only has the experimentally determined sign but is also quantitatively close to the experimental value of −10 GPa. This result suggests that also based on first-principles calculations, the 14 Å Fe film is bct rather than fct. The energy necessary for the (homogeneous) tetragonal distortion is calculated as 42 meV/atom.[54]

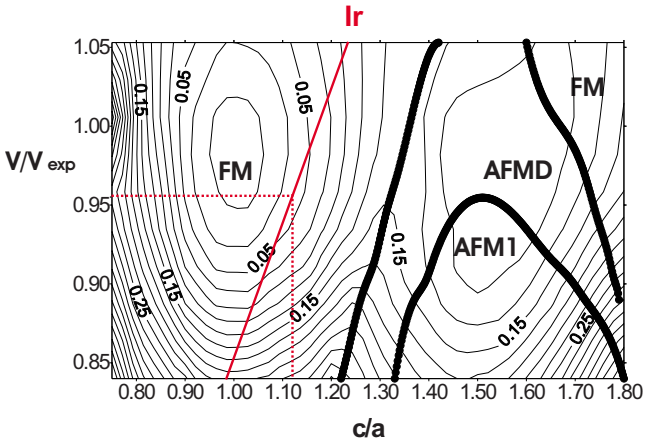


FIG. 7. (Color online) Total energy contour plot for bulk Fe as function of the $c/a_{\parallel}$ ratio and the atomic volume $V/V_{exp}$ relative to the bcc equilibrium value with $V_{exp}=11.72$ Å$^3$ [Fig. 3(a) taken from Ref. 8 by courtesy of the authors]. Contour intervals are 20 meV/atom. The thick lines are the boundaries between ferromagnetic (FM) and antiferromagnetic phases whereby AFM1 and AFMD stand for single-layer ($\uparrow\downarrow\cdots$) and double-layer ($\uparrow\uparrow\downarrow\downarrow\cdots$) antiferromagnetic states, respectively. The straight line inserted enforces the value $a_{\parallel}=2.715$ Å valid for the Ir(001)-$(1\times1)$ substrate.

Other total energy calculations along the EBP[7,8] reproduce nicely both the geometry of our thick film as well as its ferromagnetism. Figure 7 (taken from Ref. 8) displays the total energy contour lines in the epitaxial plane, where the thick lines are boundaries between different magnetic phases (see figure caption). For a fixed surface parallel lattice parameter $a_{\parallel}$, the relation between volume and $(c/a_{\parallel})$ writes as $V/V_{exp}=k(c/a_{\parallel})$, with $k=(a_{\parallel})^3/2V_{exp}$. For Ir(001)-$(1\times1)$ with $a_{\parallel}=2.715$ Å, the value $k\approx0.854$ results. The corresponding straight line is inserted in Fig. 7. The point of minimum energy along this line, as indicated by the crossing of the dotted lines, is at $c/a_{\parallel}\approx1.125$, very close to the experimental value $2d_b^{film}/a_{\parallel}(\mathrm{Ir})=1.142$. Also, the minimum is clearly within the FM phase, that is, both the structural and magnetic experimental results for the 9 ML Fe film are fully in line with theory.

Surprisingly, we find that the first two interlayer spacings nearest to the vacuum interface of the 9 ML film are expanded by $\Delta d_{12}^{film}/d_b^{film}=+2.6\%$ and $d_{23}^{film}/d_b^{film}=+1.9\%$ with respect to the bulk interlayer distance of the film (we recall that the error limits of our structure determination are of the order of 0.01 Å for the first two spacings equivalent to a relative value of about 0.6%). For the surface of a bulk material, this expansion would be rather unusual. In fact, for the (001) surface of a bulk Fe crystal, the usual contraction of the top spacing followed by an expansion of the second spacing is reported [$\Delta d_{12}/d_b=-5\%$, $\Delta d_{23}/d_b=+5\%$ (Ref. 55) and $\Delta d_{12}/d_b=-3.5\%$, $\Delta d_{23}/d_b=+3.5\%$ (Ref. 56)].

An unexpected surface expansion is frequently attributed to surface contaminations. These might originate either from impurities within the iron supply or from postadsorption from the residual gas, predominantly hydrogen. The former source appears rather unlikely since we used a highly purified Fe material, which was well degassed and in use for already quite a while. The amount of possible hydrogen uptake can be estimated from a "worst-case" analysis assuming the background to consist of hydrogen only. Since hydrogen is found to desorb from the films at about 270 K (peak maximum in separate measurements of temperature programed desorption), we start with an uncovered surface right after annealing of the film. Cooling to 90 K and LEED data acquisition took about $10^3$ s in total. With a typical pressure of $6\times10^{-11}$ mbar, an ion gauge sensitivity of 2.4 for hydrogen, and assuming the initial sticking coefficient to be $s_0=1$, the upper limit for the total hydrogen coverage results to be about 0.2 ML at the end of the LEED measurement. Yet, the real initial sticking coefficient is $s_0\approx1.5\times10^{-3}\ll1$ as measured for hydrogen adsorption on Fe(100),[57] so that our hydrogen coverage must be well below 1%. In line with that is the result of an additional LEED analysis of a 2 ML Fe film kept at a temperature of 270 K at which no hydrogen sticks at the surface. This analysis reveals an even slightly more enhanced top layer spacing of 1.66 Å compared to 1.64 Å measured at low temperature.

All these observations favor that the values of the upper two film spacings are an intrinsic feature of the film structure rather than caused by surface contamination. This might be interpreted as follows: As well known, the top layers of transition or noble metal crystals (rather than films) are under positive (=tensile) stress.[58] In particular, the top layers of bcc Fe(100) are considerably strained according to first-principles calculations.[54] The stress is caused by the redistribution of electrons upon the truncation of the bulk when the surface is created, and this charge redistribution also gives rise to the contraction of the top surface spacing. We tentatively assume that similar mechanisms may apply also for the bct phase of thicker Fe films on Ir. In our case, the tensile surface stress of Fe is released to some extent due to the smaller in-plane lattice parameter of Ir, as compared to $\alpha$-Fe. In the absence of first-principles calculations for the present case, we speculate that this is the reason for the top spacing of our film being expanded rather than contracted. Eventually, we mention that such an expansion was also reported for Fe films of comparable thickness on Pd(001).[16]

### B. Structure and stress of thinner films: 1–4 ML Fe

Certainly, from a crystallographic point of view, the distinction between fcc and bcc is doubtful for 1–2 ML. Nevertheless, our following discussion suggests that the physical properties of the 1–2 ML film are better described by what one might call a fct precursor, and not as a bct film.

In the region between 1 and 4 ML Fe on Ir(001)-$(1\times1)$, the film stress undergoes a transition from positive (tensile) to negative (compressive) stress as evident from Fig. 6. This change of sign of film stress may be interpreted as the films at 2 ML being fcc type. Subsequently, deposited Fe grows as bct phase on top of this fct precursor. For fcc Fe, Table I gives a misfit of +0.074, from which we calculate an in-plane stress of +11.4 GPa, and a layer spacing of 1.61 Å. Our measurement indicates a tensile film stress of +6 GPa for the growth of the first two Fe monolayers.

Thus, the fcc reference data and continuum elasticity reproduce the transition from compressive to tensile stress and

also the enlarged layer spacing with respect to the thicker films. However, the quantitative agreement is less satisfactory as in the case of the 9 ML film.

A possible reason for the worse agreement between experimental results and continuum elasticity may be due to the stronger contribution of interface effects on the resulting film structure. In contrast to the thicker films, the 2–4 ML films are characterized by a more pronounced variation of the individual layer spacings, as shown in Fig. 5. This variation points directly at the failure of continuum elasticity, which tacitly assumes a constant strain state throughout the film.

The evaluation of layer spacings appears to be even more affected by surface and interface contributions. So, the outermost two spacings of the 4 ML film have exactly the same values as in the 9 ML film (see Fig. 5), a clear indication that also the outermost two layers are of identical type that is bct-Fe. In contrast, the third spacing of the 4 ML film deviates remarkably from the corresponding value of the thick film. As an inner spacing of the film, it should not be or only negligibly affected by surface and interface properties but reflect the structural character of the film. While it is 1.55 Å for the thick bcc-type film, it is 1.61 Å for the 4 ML film, which is exactly the value predicted for a fcc-type film. Also, the interface layer spacing of the 4 ML film (1.76 Å) is exactly the average value of spacings for iridium and fct-Fe (1.765 Å) rather than the respective value for bct-Fe (1.72 Å). The 2 ML film owns almost the same spacing at the interface (1.77 Å) as the 4 ML film. As for the bct film, the top spacing is also expanded relative to the value in the bulk of the fct film (1.61 Å), in spite of the fact that there is a considerable tensile stress of the top layer. This might be due to the fact that all layers of the film are under that stress and that, according to first-principles calculations for fcc Fe(100) and different from bcc Fe(100), there is almost no additional stress in the top layer.[54] From this discussion, we draw the conclusion that also the layer spacings derived for the 2 and 4 ML thick films strongly corroborate the postulation of a 2 ML thick fct-Fe precursor film which grows and remains at the interface toward the iridium substrate. Finally, we recognize that the interface layer spacing of the 1 ML film fails to fit into the above presented scheme. Yet, this "film" has to be regarded much more as an adsorbate than a film, as there are no Fe nearest-neighbor bonds at all. This interpretation is also in line with the observation that in this case, only the Ir substrate exhibits remarkable changes of its relaxation profile.

Interestingly, molecular dynamics calculations for freestanding Fe films show that with decreasing film thickness, the bcc(100) phase becomes unstable and undergoes a transition to the fcc(100) phase by a shrinking of the in-plane and an expansion of the vertical lattice parameter.[54] The authors suggest that the driving force for the martensitic transformation from bcc to fcc is the softening of the elastic constant $c_{33}$ with decreasing thickness. This scenario fits to the interpretation that our low coverage films are of fct type (the bcc $\rightarrow$ fcc transition occurs also for 3 and 4 ML freestanding films,[54] but this may be inhibited in our case by the epitaxial constraints).

### C. Comparison to Fe/Rh(001) and Fe/Ir multilayers

Finally, we compare our results of the Fe-Ir system to those obtained previously for Fe growth on Rh(001).[18,19] The lattice constant of Rh is 3.80 Å,[19] which is very close to the value of Ir (3.839 Å). Thus, one might speculate that the similar epitaxial misfit will lead to a comparable film structure. Indeed, pseudomorphic growth of Fe has been found for up to ten layers on Rh.[18] Thicker films of 8–10 layers have been identified as bct Fe, in agreement with our results on thicker films. The layer spacing of the bilayer film has been reported to be expanded with respect to that of the thicker film. Again, this finding is in line with our results on the 2 ML film. The magnetic properties of Fe on Rh(001) have been studied by MOKE at 80 K, and the authors report that no magnetic signal could be obtained up to 6 ML, and thicker films show a magnetic response.[19] These findings are qualitatively in agreement with our magnetic studies, where we succeed in getting a magnetic response for films as thin as four layers. The authors propose the role of a fct phase with an antiferromagnetic order for the suppression of a ferromagnetic response.

Ir buffer films grown on MgO(001) have been used before to study the structure and magnetism of Ir/Fe superlattices.[59–61] This previous work identified fcc Fe on Ir(001) below five layers. The roughening of the interface at higher thickness led to a loss of pseudomorphic growth, and this limits the equivalence between the previous superlattice study and our work on a bulk Ir crystal.

## V. CONCLUSION

The combined application of structural analysis by quantitative LEED with stress measurements by the cantilever bending technique reveals a subtle interplay between structure and stress of Fe monolayers.

Stress measurements are sensitive to the film thickness integrated over all stresses within the film. As such, they provide a reliable indication for the range of pseudomorphic growth and for structural transitions during growth. In connection with the highly accurate LEED structure analysis, we obtain both the in-plane and out-of-plane strains of the film and the resulting stress of a given structure. This combination allows us to distinguish between different reference states in order to identify strained Fe films as fct or bct.

In conclusion, we propose a structural model of the Fe-Ir system, which exhibits pseudomorphic growth from 0–10 ML. Our analysis suggests that the first two Fe layers, which grow on top of the Ir substrate, are a fct precursor. It is characterized by an increased layer spacing as compared to thicker films and by a tensile film stress. With increasing film thickness, Fe grows in its bct phase on top of the fct precursor. Thicker films are considerably compressed in plane by −5.3%. The films are under a compressive stress of −10 GPa and show ferromagnetic behavior with an easy in-plane magnetization direction. The deposition of thicker films leads to the formation of misfit dislocations, which lead to a strain and stress relaxations.

**ACKNOWLEDGMENTS**

The authors from Erlangen are indebted to the Deutsche Forschungsgemeinschaft (DFG) for financial support. C.G. is grateful for stipends by the Alexander von Humboldt-Stiftung and by the European Commission through its Marie Curie Intra-European Programme. Special thanks are due to M. Friák, M. Šob, and V. Vitek for providing us Fig. 3(a) of their paper[8] and for the permission to use it in the present paper.

[1] M. Wuttig and X. Liu, *Ultrathin Metal Films*, Springer Tracts in Modern Physics Vol. 206 (Springer, Berlin, 2002), Chap. 6.
[2] D. Sander, Rep. Prog. Phys. **62**, 809 (1999).
[3] V. L. Moruzzi, P. M. Marcus, and J. Kübler, Phys. Rev. B **39**, 6957 (1989).
[4] P. Alippi, P. M. Marcus, and M. Scheffler, Phys. Rev. Lett. **78**, 3892 (1997).
[5] P. M. Marcus and P. Alippi, Phys. Rev. B **57**, 1971 (1998).
[6] S. L. Qiu, P. M. Marcus, and H. Ma, J. Appl. Phys. **87**, 5932 (2000).
[7] S. L. Qiu, P. M. Marcus, and H. Ma, Phys. Rev. B **64**, 104431 (2001).
[8] M. Friák, M. Šob, and V. Vitek, Phys. Rev. B **63**, 052405 (2001).
[9] P. M. Marcus, F. Jona, and S. L. Qiu, Phys. Rev. B **66**, 064111 (2002).
[10] M. Stampanoni, A. Vaterlaus, M. Aeschlimann, and F. Meier, Phys. Rev. Lett. **59**, 2483 (1987).
[11] H. Li and B. P. Tonner, Phys. Rev. B **40**, 10241 (1989).
[12] H. Li, Y. S. Li, J. Quinn, D. Tian, J. Sokolov, F. Jona, and P. M. Marcus, Phys. Rev. B **42**, 9195 (1990).
[13] S. H. Lu, Z. Q. Wang, D. Tian, Y. S. Li, F. Jona, and P. M. Marcus, Surf. Sci. **221**, 35 (1989).
[14] W. L. O'Brien and B. P. Tonner, Phys. Rev. B **52**, 15332 (1995).
[15] B. Schirmer and M. Wuttig, Phys. Rev. B **60**, 12945 (1999).
[16] J. Quinn, Y. S. Li, H. Li, D. Tian, F. Jona, and P. M. Marcus, Phys. Rev. B **43**, 3959 (1991).
[17] J. R. Childress, R. Kergoat, O. Durand, J.-M. George, P. Galtier, J. Miltat, and A. Schuhl, J. Magn. Magn. Mater. **130**, 13 (1994).
[18] A. M. Begley, S. K. Kim, J. Quinn, F. Jona, H. Over, and P. M. Marcus, Phys. Rev. B **48**, 1779 (1993).
[19] C. Hwang, A. K. Swan, and S. C. Hong, Phys. Rev. B **60**, 14429 (1999).
[20] N. Nakayama, T. Okuyama, and T. Shinjo, J. Phys.: Condens. Matter **5**, 1173 (1993).
[21] A. M. Begley, S. K. Kim, F. Jona, and P. M. Marcus, Phys. Rev. B **48**, 1786 (1993).
[22] V. Blum *et al.*, Phys. Rev. B **59**, 15966 (1999).
[23] F. Baudelet, M.-T. Lin, W. Kuch, K. Meinel, B. Choi, C.-M. Schneider, and J. Kirschner, Phys. Rev. B **51**, 12563 (1995).
[24] B. Feldmann, B. Schirmer, A. Sokoll, and M. Wuttig, Phys. Rev. B **57**, 1014 (1998).
[25] B. Schirmer, B. Feldmann, and M. Wuttig, Phys. Rev. B **58**, 4984 (1998).
[26] F. Bruno *et al.*, Phys. Rev. B **66**, 045402 (2002).
[27] W. A. A. Macedo, F. Sirotti, G. Panaccione, A. Schatz, W. Keune, W. N. Rodrigues, and G. Rossi, Phys. Rev. B **58**, 11534 (1998).
[28] L. Hammer, S. Müller, and K. Heinz, Surf. Sci. **569**, 1 (2004).
[29] J. Thomassen, F. May, B. Feldmann, M. Wuttig, and H. Ibach, Phys. Rev. Lett. **69**, 3831 (1992).
[30] A. Ignatiev, A. Jones, and T. Rhodin, Surf. Sci. **30**, 573 (1972).
[31] A. Schmidt, W. Meier, L. Hammer, and K. Heinz, J. Phys.: Condens. Matter **14**, 12353 (2002).
[32] L. Hammer, W. Meier, A. Schmidt, and K. Heinz, Phys. Rev. B **67**, 125422 (2003).
[33] A. Klein, A. Schmidt, L. Hammer, and K. Heinz, Europhys. Lett. **65**, 830 (2004).
[34] J. Küppers and H. Michel, Appl. Surf. Sci. **3**, 179 (1979).
[35] K. Heinz, G. Schmidt, L. Hammer, and K. Müller, Phys. Rev. B **32**, 6214 (1985).
[36] D. Lerch, A. Klein, A. Schmidt, S. Müller, L. Hammer, K. Heinz, and M. Weinert, Phys. Rev. B **73**, 075430 (2006).
[37] K. Heinz, Rep. Prog. Phys. **58**, 637 (1995).
[38] V. Blum and K. Heinz, Comput. Phys. Commun. **134**, 392 (2001).
[39] J. B. Pendry, *Low Energy Electron Diffraction* (Academic, London, 1974).
[40] J. Rundgren, Phys. Rev. B **68**, 125405 (2003).
[41] M. Kottcke and K. Heinz, Surf. Sci. **376**, 352 (1997).
[42] J. Pendry, J. Phys. C **13**, 937 (1980).
[43] D. Sander and J. Kirschner, Appl. Phys. A: Mater. Sci. Process. **87**, 419 (2007).
[44] D. Sander, S. Ouazi, V. Stepanyuk, D. Bazhanov, and J. Kirschner, Surf. Sci. **512**, 281 (2002).
[45] D. Sander and H. Ibach, *Adsorbed Lagers on Surfaces. Part 2: Measuring Techniques and Surface Properties Changed by Adsorption*, Landolt-Börnstein, New Series, Group III, Vol. 42, Pt. A2 (Springer, Berlin, 2002), Chap. 4.4, pp. 4.4-1–4.4-49.
[46] D. Sander, A. Enders, and J. Kirschner, Europhys. Lett. **45**, 208 (1999).
[47] *Crystal Data*, edited by J. Donnay and H. Ondik (National Bureau of Standards, Gaithersburg, MD, 1973).
[48] R. F. S. Hearmon, *The Elastic Constants of Non-Piezoelectric Crystals*, Landolt-Börnstein, New Series Group III, Vol. 2 (Springer-Verlag, Berlin, 1969).
[49] J. Zarestky and C. Stassis, Phys. Rev. B **35**, 4500 (1987).
[50] J. Adams, D. Agosta, R. Leisure, and H. Ledbetter, J. Appl. Phys. **100**, 113530 (2006).
[51] D. Sander, W. Pan, S. Ouazi, J. Kirschner, W. Meyer, M. Krause, S. Müller, L. Hammer, and K. Heinz, Phys. Rev. Lett. **93**, 247203 (2004).
[52] R. Mahesh, D. Sander, S. M. Zharkov, and J. Kirschner, Phys. Rev. B **68**, 045416 (2003).
[53] W. Pan, D. Sander, M. T. Lin, and J. Kirschner, Phys. Rev. B **68**, 224419 (2003).
[54] W. S. Lai and X. S. Zhao, Appl. Phys. Lett. **85**, 4340 (2004).
[55] Z. Q. Wang, Y. S. Li, F. Jona, and P. M. Marcus, Solid State Commun. **61**, 623 (1987).
[56] R. L. Headrick, P. Konarski, S. M. Yalisove, and W. R. Graham, Phys. Rev. B **39**, 5713 (1989).
[57] H. F. Berger and K. D. Rendulic, Surf. Sci. **251/252**, 882 (1991).

[58] H. Ibach, Surf. Sci. Rep. **29**, 193 (1997).
[59] S. Andrieu, M. Piecuch, L. Hennet, J. Hubsch, and E. Snoeck, Europhys. Lett. **26**, 189 (1994).
[60] A. Traverse, S. Pizzini, S. Andrieu, A. Fontaine, and M. Piecuch, Surf. Sci. **319**, 131 (1994).
[61] S. Andrieu, F. Lahatra Razafindramisa, E. Snoeck, H. Renevier, A. Barbara, J. M. Tonnerre, M. Brunel, and M. Piecuch, Phys. Rev. B **52**, 9938 (1995).